Evaluation of differential absorption radars in the 183 GHz band for profiling water vapour in ice clouds

Alessandro Battaglia[1,2] and Pavlos Kollias[3,4]

[1]Department of Physics and Astronomy, University of Leicester, Leicester, UK
[2]National Centre for Earth Observation, UK
[3]Stony Brook University, NY, USA
[4]University of Cologne, Cologne, Germany

Correspondence: Alessandro Battaglia
ab474@le.ac.uk

Abstract. Relative humidity (RH) measurements in ice clouds are essential for determining the ice crystals growth processes and rates. A differential absorption radar (DAR) system with several frequency channels within the 183.3 GHz water vapor absorption band is proposed for measuring RH within ice clouds. Here, the performance of a DAR system is evaluated by applying a DAR simulator to A-Train observations in combination with collocated European Centre for Medium-Range Weather Forecasts (ECMWF) reanalysis. Observations from the CloudSat W-band radar and from the CALIPSO lidar are converted first into ice microphysical properties and then coupled with ECMWF temperature and relative humidity profiles in order to compute scattering properties at any frequency within the 183.3 GHz band. Self-similar Rayleigh Gans approximation is used to model the ice crystal scattering properties. The radar reflectivities are computed both for a space-borne and a ground-based DAR system by using appropriate radar receiver characteristics. Sets of multi-frequency synthetic observation of attenuated reflectivities are then exploited to retrieve profile of water vapour density by fitting the line shape at different levels. 10 days of A-Train observations are used to test the measurement technique performance for different combination of tones when sampling ice clouds globally. Results show that that water vapour densities can be derived with accuracies that can enable ice process studies (i.e. better than 3%) both from a ground-based system (at the minute temporal scale and with circa 100 m vertical resolution) and from a space/airborne system (at 500 m vertical resolution and with circa 5 km integration lengths) with four tones in the right wing of the absorption line. A ground-based DAR system to be deployed at high latitude/high altitudes is highly recommended to test the findings of this work in the field.

1 Introduction

Adequate understanding of the cloud and precipitation processes that contribute to Earth's water and energy cycle is required before significant progress occur in our ability to predict future climate scenarios. This calls for a paradigm shift away from the current observing system that mainly capture snapshots of "states" to the next-generation of observing systems that can observe both states and "processes" (Stephens et al., 2018).

Future space-borne cloud and precipitation radars are expected to be at the center of such a revolution (The Decadal Survey, 2017), thus enhancing the view depicted in the past 20 years by the TRMM Ku-band Precipitation radar (Kummerow et al., 1998), the GPM Dual-frequency (Ku-Ka) Precipitation Radar (Skofronick-Jackson et al., 2016) and the CloudSat W-band Cloud Profiling Radar (Tanelli et al., 2007). While the first Doppler radar is expected to be launched on board the EarthCARE

5   satellite in 2021 (Illingworth et al., 2015) innovative radar concepts have been studied in the past decade ranging from multi-wavelength radars proposed e.g. as payloads of the Aerosol/Cloud/Ecosystems (ACE) mission and the Polar Precipitation Measurement (PPM) mission for microphysical studies (Leinonen et al., 2015; Joe et al., 2010; Durden et al., 2016; Tanelli et al., 2018) to Doppler radars for understanding cloud dynamics (Battaglia and Kollias, 2014; Illingworth et al., 2018; Battaglia et al., 2018; Kollias et al., 2018) to constellations of radars in a CubeSat for advancing convective parameterizations (Peral et al.,

10   2015; Haddad et al., 2017; Sy et al., 2017).

In parallel, radar systems operating at much higher frequencies such as the G-band (110-300 GHz) have been proposed to study ice/snow microphysical properties (Hogan and Illingworth, 1999; Battaglia et al., 2014). Furthermore, there is interest in exploring the possibility of profiling the water vapor in cloudy areas (Lebsock et al., 2015; Millán et al., 2016; Roy et al., 2018) by using differential absorption radar (DAR) measurements near the 183.3 GHz water vapor absorption line. Water vapor is

15   one of the most critical atmospheric variables for numerical weather prediction models (Millán et al. (2016)) and profiles of humidity in cloudy areas are not adequately measured by current or planned systems as stated by WMO (Anderson, 2014; Nehrir et al., 2017). While Lebsock et al. (2015) theoretically investigated the possibility of profiling water vapor within the cloudy boundary layer in presence of cumulus and stratocumulus clouds and of quantifying integrated column water vapor over ocean surfaces with a DAR system with channels on the left wing of the 183.3 GHz absorption line, Millán et al. (2016)

20   examined how the DAR technique can be applied to water vapor sounding in clouds at all levels by adopting multiple tones within the whole absorption band (140 to 200 GHz). Recently the DAR technique within the G-band has been demonstrated by Cooper et al. (2018): not only ground-based measurements of planetary-boundary-layer clouds have been performed but an error model and an inversion algorithm have been developed for retrieving the water vapor profile as well (Roy et al., 2018).

This work aims at assessing the potential of both space-borne and ground-based DAR systems for ice cloud studies. When

25   coupled with that of temperature the knowledge of the water vapor density in ice clouds has two benefits.

    1. It allows to derive the relative humidity with respect to ice (RH_i) and then to identify regions where depositional growth/sublimation processes are dominant (i.e. when the supersaturation is positive/negative in Fig. 1). Particle growth by deposition is an important growth process in cold environments particularly when supercooled liquid water layers provide sufficient water vapor for rapid growth (i.e. in regions above the dashed blue line in Fig. 1). DAR observations

30   could complement polarimetric radar observations like differential reflectivity that are particularly sensitive to depositional growth in temperature regions which favor growth of asymmetric particle shapes (e.g. Verlinde et al. (2013); Oue et al. (2016)).
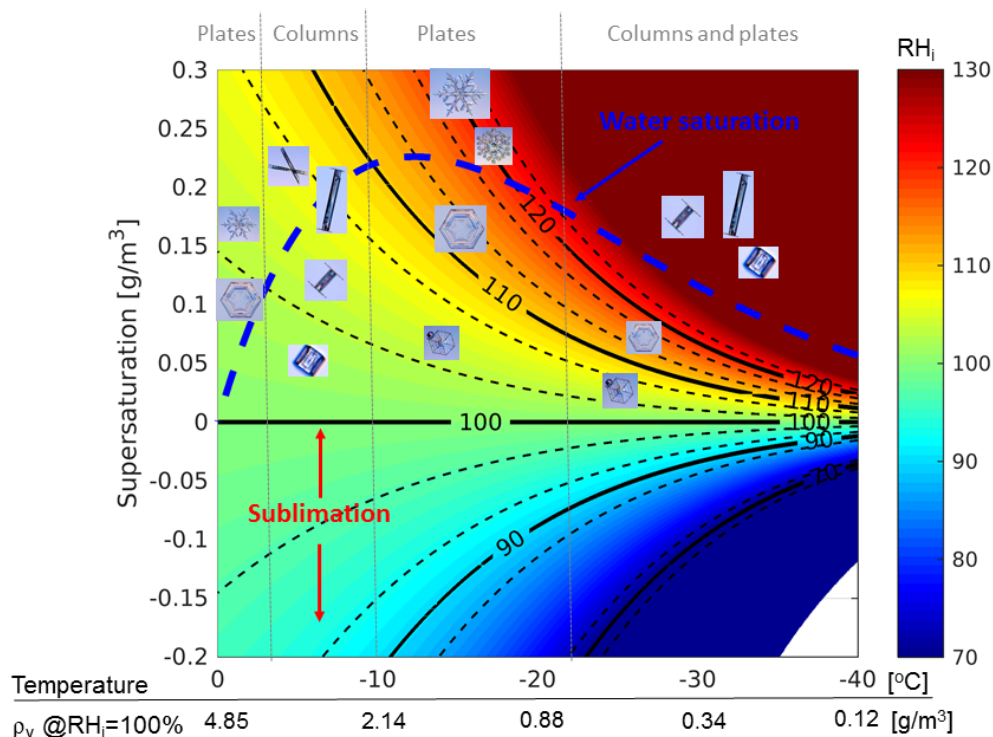
Figure 1. Dominant ice crystal habits (small photographs) as suggested by Magono and Lee (1966) for different environmental conditions as classified in terms of temperature (x-axis) and supersaturation (y-axis). The color maps the relative humidity with respect to ice, RH_i. The dashed blue line indicates the supersaturation of supercooled water relative to ice. Black lines correspond to different level of RH_i as indicated by the labels. The dashed lines surrounding each continuous line correspond to a $\pm 3\%$ change in RH_i.

2. The detection and the description of supersaturation areas in high level ice clouds could help us understand how the ice crystal grow significantly enhance water mass fluxes due to sedimentation. This could have an impact on the dehydration of the air entering the lower stratosphere (Kärcher et al., 2014).

3. It allows to identify dominant ice crystal habit growth in the different portions of the clouds as suggested by Magono and Lee (1966) and schematically depicted in Fig. 1. Since the shape and internal mass distribution of the ice particles is affecting their scattering properties this has an immediate impact onto improving remote sensing retrievals.

The water vapor density for a given relative humidity is a strong function ot temperature: for instance for $RH_i = 100\%$ the water vapor density is changing by more than one order of magnitude (from 4.85 to 0.34 g/m³, see x-axis in Fig. 1) when

moving from 0 to $-30°C$. A knowledge of RH_i within 3% seems appropriate for identifying the relevant regimes in Fig. 1. This highlights that, in order to retrieve useful information for ice cloud studies, water vapor densities must be retrieved with good accuracy ($\sim 3\%$ or better) for a range of values between 0.5 and 5 g/m^3.

The paper is structured as following: first the theory of water vapor retrieval with DAR is shortly revisited (Sect. 2). In Sect. 3
5   CloudSat observations are used to reconstruct realistic ice microphysics profiles that can be used as input in a forward model for simulating reflectivities profiles at any frequency in the G-band.

Conclusions and future work are presented in Sect. 5.

2   Theory of water vapor retrievals

Here the theory underpinning DAR, thoroughly covered in Lebsock et al. (2015); Millán et al. (2016); Roy et al. (2018), is
10   briefly revised. The measured reflectivity from target with effective reflectivity $Z_e(r,f)$ at a given range r is given by:

$$Z_{meas}(r,f) = Z_e(r,f)\, e^{-2\tau(0\to r,f)} \tag{1}$$

where $\tau(0 \to r,f)$ is the one way optical depth from the radar to the range r. The exponential term accounts for the radar attenuation due to the gases and the hydrometeors with the factor two accounting for the two way path of the radar wave. Note that multiple scattering effects (Battaglia et al., 2010) will be neglected hereafter since they are minimized by the small radar
15   footprints and by the low single scattering albedo of the medium at frequency in the vicinity of the absorption line. Following Roy et al. (2018) we consider the ratio of measured reflectivities at two ranges r_1 and $r_2 = r_1 + \Delta r$:

$$\frac{Z_{meas}(r_1,f)}{Z_{meas}(r_2,f)} = \frac{Z_e(r_1,f)}{Z_e(r_2,f)}\, e^{-2[\tau(0\to r_1,f)-\tau(0\to r_2,f)]} = \frac{Z_e(r_1,f)}{Z_e(r_2,f)}\, e^{2\langle k_e(f)\rangle_{\Delta r}\Delta r} \tag{2}$$

where the $\langle\rangle_{\Delta r}$ symbol corresponds to taking the mean value for ranges between r_1 and r_2 so that

$$\langle k_e(f)\rangle_{\Delta r} \equiv \frac{\tau(0\to r_2,f)-\tau(0\to r_1,f)}{\Delta r} = \frac{\int_{r_1}^{r_2} k_e(r,f)dr}{\Delta r} = \frac{\int_{r_1}^{r_2}[k_{e\,gas}(r,f)+k_{e\,hydro}(r,f)]\,dr}{\Delta r} \tag{3}$$

20   is the mean extinction coefficient for such ranges. This equation can be further simplified by separating the water vapour components from the other gases and introducing the water vapour absorption coefficient per unit mass, κ_v as:

$$\langle k_e(f)\rangle_{\Delta r} = \langle\rho_v\kappa_v(f,p,T)\rangle_{\Delta r} + \langle k_{e\,dry\,air+hydro}(f)\rangle_{\Delta r} \approx \langle\rho_v\rangle_{\Delta r}\kappa_v(f,\langle p\rangle_{\Delta r},\langle T\rangle_{\Delta r}) + \langle k_{e\,dry\,air+hydro}(f)\rangle_{\Delta r} \tag{4}$$

where in the last step we have assumed that the line shape $\kappa_v(f)$ within the Δr-layer can be approximated by its value at the mean temperature and pressure of the layer and we have conjoined the dry air and hydrometeor extinction.

25   If we invert Eq. (3) we can then write:

$$\langle k_e(f)\rangle_{\Delta r} = \frac{1}{2\Delta r}\log\left(\frac{Z_{meas}(r_1,f)}{Z_{meas}(r_2,f)}\frac{Z_e(r_2,f)}{Z_e(r_1,f)}\right) \tag{5}$$

and recombining Eq. (5) and Eq. (4) we finally get:

$$\gamma(f,r_1,r_2) \equiv \frac{1}{2\Delta r}\log\left(\frac{Z_{meas}(r_1,f)}{Z_{meas}(r_2,f)}\right) = \langle\rho_v\rangle_{\Delta r}\kappa_v(f,\langle p\rangle_{\Delta r},\langle T\rangle_{\Delta r}) + \underbrace{\langle k_{e\,dry\,air+hydro}(f)\rangle_{\Delta r} - \frac{1}{2\Delta r}\log\left(\frac{Z_e(r_2,f)}{Z_e(r_1,f)}\right)}_{A+Bf}$$

$$(6)$$

The DAR rationale is based on the idea that by performing measurements of the left hand side of Eq. (6) at different frequencies it will be possible to fit the terms on the right hand side. The first term is directly proportional to the water vapor density via the line shape $\kappa_v(f)$; the last two terms are related to the dry air plus hydrometeor attenuation and the effective reflectivity ratio

5   at the two ranges (thus affected by the vertical variability). They can be assumed to vary weakly with frequency. Extinction of supercooled droplet is indeed proportional to frequency (e.g. see Lhermitte (1990)) and ice crystals behaves similarly with a slight linear increase with frequency, as demonstrated in Fig. 2. Therefore the last two terms are modelled in this study via a dependence which is linear with frequency. Since the the line shape $\kappa_v(f)$ is known at a given T and p then $\langle \rho_v \rangle_{\Delta r}$ can be derived by a mean square fitting procedure which fits all three terms on the right in Eq. (6) to the measured γ terms. The

10   procedure also allows the computation of errors for the retrieved fitted parameters and of a quality index for the fitting via the normalised χ^2. If only three tones are available (or the full range of tones is less than 10 GHz) then B is assumed to be equal 0 (as done in Roy et al. (2018)). Therefore when only two tones are available ρ_v and its error can be directly computed from formula (12) and (13) in Roy et al. (2018). Note that the quantities $\gamma(f, r_1, r_2)$ are not affected by absolute calibration, which makes the whole procedure immune to calibration errors.

15   3   Simulation of DAR profiles from CloudSat data

At present, no radar reflectivity measurements at multiple G-band tones are available that can be used to evaluate the performance of the technique. Our approach relies on using retrieved ice microphysical properties from spaceborne sensors and use them as input to a forward radar model (DAR model) to generate reflectivities around the 183.3 GHz absorption band.

    The CloudSat 94 GHz (3.2 mm) Cloud Profiling Radar (CPR) provides global observations of ice cloud profiles at a vertical

20   resolution of 480 m and a cross-track/along-track horizontal footprint of 1.5 km×2.5 km (Tanelli et al., 2008). When integrated with the observations from the CALIPSO Cloud-Aerosol Lidar with Orthogonal Polarization (CALIOP) (Winker et al., 2007) such observations can be used to retrieve ice microphysics. Here retrievals adopting the DARDAR algorithm (Delanoë and Hogan (2010), http://www.icare.univ-lille1.fr/projects/dardar/) are used as input for the the DAR modelling. ECMWF auxiliary data are used as input for temperature, pressure and relative humidity.

25   The DAR forward model uses the millimeter-wave propagation model from Rosenkranz (1999) for gas attenuation whereas the self-similar Rayleigh-Gans scattering model (Hogan and Westbrook, 2014) is adopted for computing the scattering properties of ice particles. The ice crystals model proposed by Leinonen and Szyrmer (2015) and labelled as model "A; $LWP = 0.1 kg/m^2$" is used. Tridon et al. (2019) have shown that this scattering model generally well fits triple frequency radar measurements and in situ measurements.

30   Noise is injected into the reflectivity measurements according to the formula (see Appendix in Hogan et al. (2005)):

$$\Delta Z[dB] = \frac{4.343}{\sqrt{N_p}} \left[max\left(1, \frac{\lambda}{4\sqrt{\pi}\sigma_v\tau_s}\right) + \frac{2}{SNR} + \frac{1}{SNR^2} \right]^{1/2} \qquad (7)$$
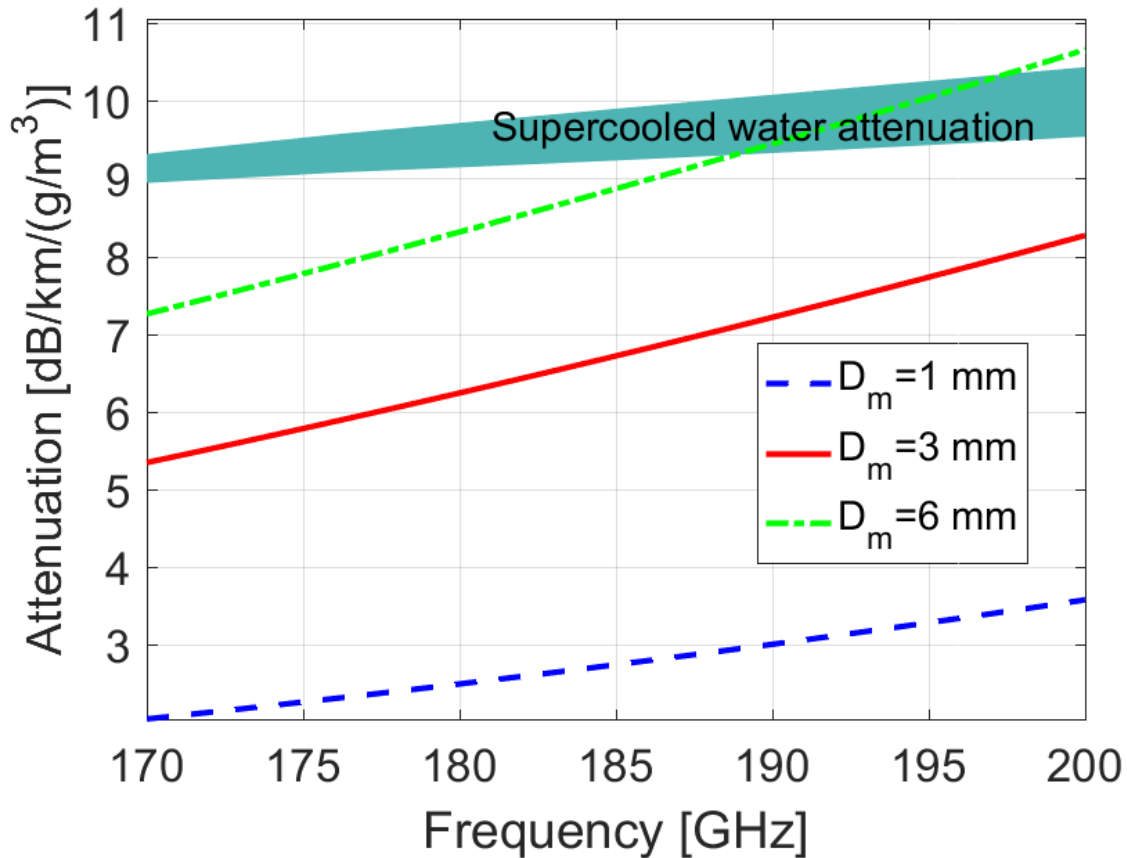
Figure 2. Attenuation coefficient for ice crystals with different mass-weighted maximum particle diameters as indicated in the legend for the frequency range of interest for this study. The model "A; $LWP = 0.1 kg/m^2$" from Leinonen and Szyrmer (2015) is used. The shaded area corresponds to the attenuation coefficient for supercooled liquid clouds for temperatures in the range between $-30°C$ and $0°C$.

where N_p is the number of radar pulses transmitted (e.g. in the space-borne configuration 4200 for an integration length of 5 km), τ_s is the time between samples (i.e. the reciprocal of the pulse repetition frequency) and σ_v is the spectral width of the Doppler spectrum. For space-borne systems the first term inside the bracket is practically always close to one because the Doppler spectral width is expected to exceed 2 m/s due to the large satellite velocity (see Eq. 6 in Battaglia and Kollias (2014)).

5   The first term inside the square bracket needs to be at least one because the number of independent samples has to be smaller or equal to the number of samples. This implies that the so-called "time to independence" is of the order of 100 μs, thus smaller than the time between pulses (equal to 166.7 μs for a PRF=6 kHz). The single pulse sensitivity is assumed to be -22 dBZ, a realistic value with current technology (see Tab. 1). For ground-based system on the other hand we have assumed a spectral width equal to 1 m/s and a single pulse sensitivity of -50 dBZ at 1 km range with 1 s integration (see Tab. 2). In all cases we

Table 1. Technical specifications of the DAR space-borne system used in this study. The configuration here adopted is the one proposed in an on-going UK-CEOI study (Dr Duncan Robertson, personal communications).

Satellite altitude, h_{sat}	500 km
Satellite velocity, v_{sat}	7600 ms^{-1}
Frequency	170-200 GHz
Transmit power	100 W (EIK technology)
Antenna diameter	≥ 2 m
Antenna beam-width, θ_{3dB}	$\leq 0.05°$
Antenna gain	70 dBi
Receiver Noise Figure	6 dB
Pulse width	3.3 μs
Pulse Repetition Frequency (with frequency diversity)	6 kHz
Single pulse sensitivity	-22 dBZ

Table 2. Specifics of the frequency-modulated-continuous wave radar based on W-band power amplifier and GaAs Schottky diode frequency multiplication (Nils et al. (2017)) for the ground-based simulation (Dr Peter Huggard, personal communications).

Frequency	170-200 GHz
Transmit power	200 mW
Antenna diameter	0.4 m
Antenna beam-width, θ_{3dB}	$\leq 0.3°$
Antenna gain	55 dBi
Receiver Noise Figure	6.5 dB
Chirp Repetition Frequency	6 kHz
Bandwidth	2 MHz
Range resolution	75 m
Minimum detectable reflectivity @1km range and 1 s integration	-50 dBZ

assume that the sensitivity remains the same when adding more tones. This could be realized by using frequency diversity and increasing the duty cycle of the radar. A configuration where the duty cycle remains constant will also be discussed later in Sect. 4.

3.1 Case study

5 The methodology is demonstrated for a precipitating system observed by CloudSat over the Southern Ocean between Antarctica and South America on the 2nd January 2007 at about 20:16 UTC. The system extends for roughly 1300 km with temperature at the surface ranging from 281 K at the southern edge of the system to 274 K at the the northern edge of the system. The
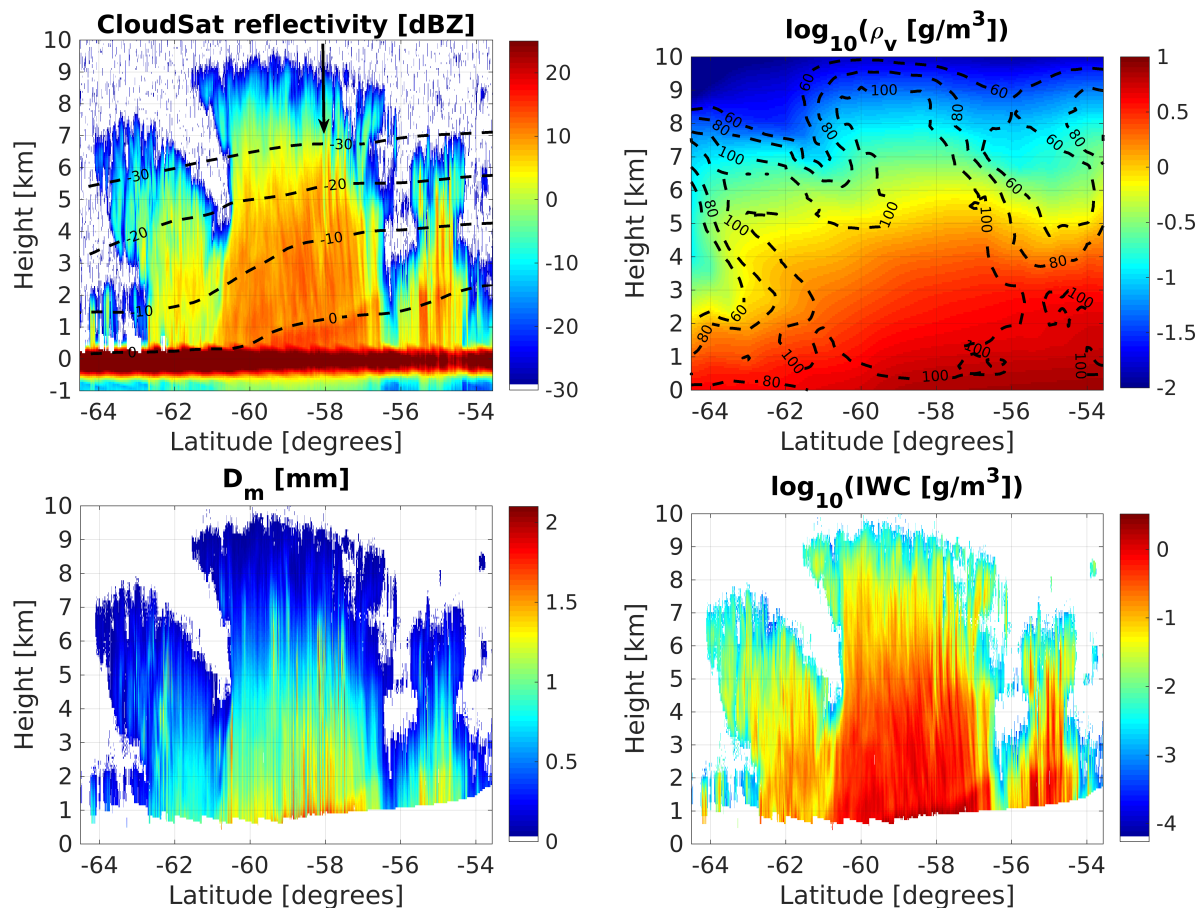
Figure 3. Top left: CloudSat measured reflectivity in the Southern Ocean south-west of Cape Horn. Dashed black lines corresponds to different isotherms as labeled while the black arrow corresponds to the profile analysed in Fig. 5. Top right: water vapor density as derived from ECMWF reanalysis with regions of constant relative humidity with respect to ice depicted as dashed lines. Bottom panels: mean mass-weighted diameter of ice particle (left) and ice water content (right) as retrieved by the DARDAR product.

CloudSat 94 GHz reflectivity as derived from the 2B-GEOPROF product (Mace et al., 2007) is shown on the top left panel of Fig. 3. The zero isotherm clearly demarcates the ice vs the liquid transition. The co-located ECMWF reanalysis for the relative humidity field with respect to ice is depicted in the top right panel. In the glaciated region of the precipitating system the synergy between the CloudSat radar and the CALIPSO lidar (Sassen et al., 2008) offers a unique prospective on the ice

5 microphysics (Battaglia and Delanöe, 2013). The outputs of the DARDAR retrieval (Delanoë and Hogan, 2010) are shown in the bottom panels of Fig. 3.

These microphysical outputs are then used with look-up-tables generated from scattering models to compute reflectivities at any frequency within the 183.3 GHz absorption line. An example of two frequencies (187 and 200 GHz) for the space-
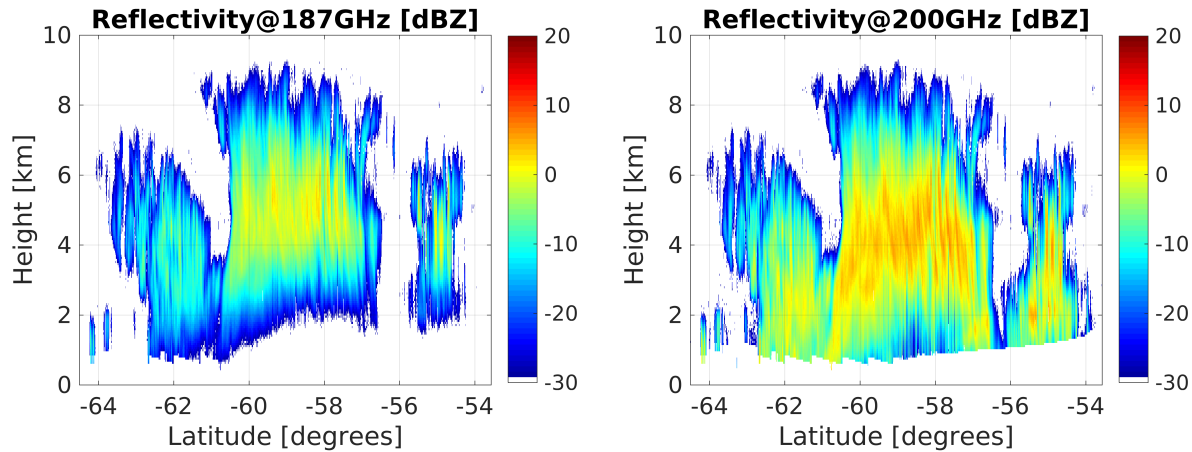
Figure 4. Simulated reflectivities at 187 and 200 GHz for a space-borne systems with specifics as in Tab. 1 for the scene shown in Fig. 3.

borne configuration is shown in Fig. 4. It is interesting to note how differently the two frequencies are penetrating into the precipitating system, with the 187 GHz severely attenuated by water vapour below 4 km. On the other hand the 200 GHz is severely attenuated in the region below 2 km at latitudes between -60° and $-58°$, a combined result of large ice water and water vapor contents.

5   The profile at latitude -58.07° (black arrow in the top left panel of Fig. 3) is used here to demonstrate how to derive a water vapor profile in a three-step procedure (see Fig. 5):

1. an interval Δr is selected and the profiles of the quantity $\gamma(f_j, r)$ [see Eq. (6)] are computed with their corresponding errors]computed from the estimated errors on the measured reflectivities via Eq. (7)] at the different DAR frequencies $f_1, f_2, \ldots$ (continuous blue lines with bars in the small insets of Fig. 5);

10   2. the spectral dependence of the line shape $\kappa_v(f, \langle p \rangle_{\Delta r}, \langle T \rangle_{\Delta r})$ is derived at each level (dashed red lines in the small insets of Fig. 5) by using the average temperature and pressure of the layer and the gas absorption model;

3. a mean square fitting procedure of the form expressed in Eq. (6) which accounts for the errors in $\gamma(f_j, r)$ allows to retrieve estimates of the three fitting parameters ($\hat{A}, \hat{B}$ and $\langle \hat{\rho_v} \rangle_{\Delta r}$). γ values that are too noisy are excluded from the fitting (e.g. at 2.76 km only four tones are considered for the space-borne configuration).

15 For the space-borne configuration the retrieval shows that a set of 7-tone DAR with frequencies on the right wing of the 183.3 GHz band as listed in the legend of the top panel of Fig. 5 can retrieve water vapor within the ice cloud with good accuracy (i.e. within 15%) between 7.0 km (240 K) down to 2.5 km (268 K) with water vapour contents changing by more than one order of magnitude.
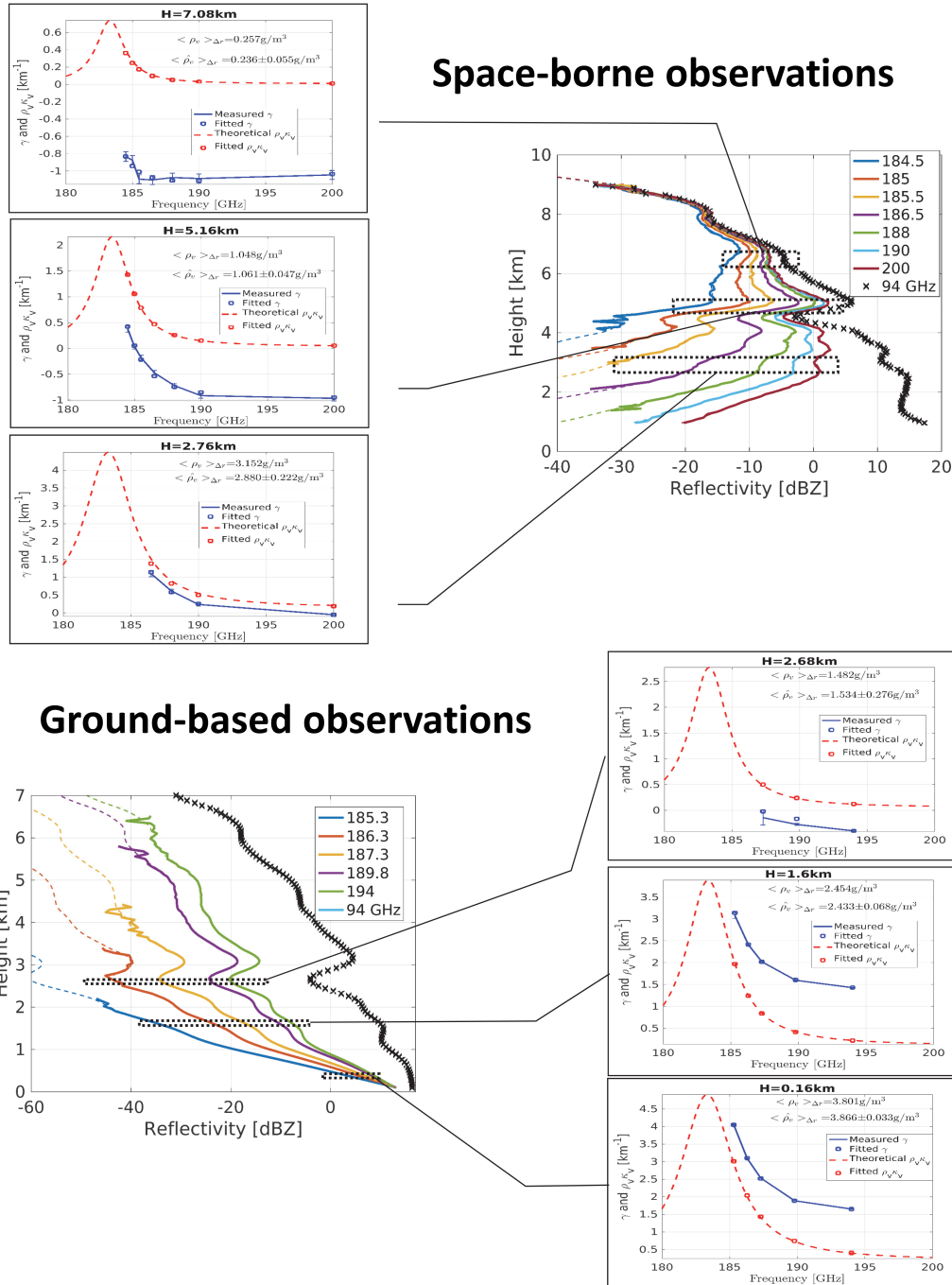
Figure 5. Top panel: simulated reflectivities for the profile at latitude -58.07° (black arrow in the top left panel of Fig. 3) for a 7-channel space-borne DAR with frequencies on the right wing of the 183.3 GHz line. An integration length of 1.1 km is assumed (corresponding to $N_p = 920$). The CloudSat 94 GHz profiles is shown for reference as well (black crosses). Continuous (dashed) lines correspond to reflectivities including (without) noise. Three panels: examples of the fitting procedure at three different altitudes to estimate $\langle \rho_v \rangle_{\Delta r}$ with $\Delta r = 500\,m$. True and estimated values are inserted in the figure. Bottom panel: same as top panel side for a 5-tone ground-based DAR. An integration time of 2 min (corresponding to $N_p = 720,000$) and a vertical resolution of 120 m are assumed.
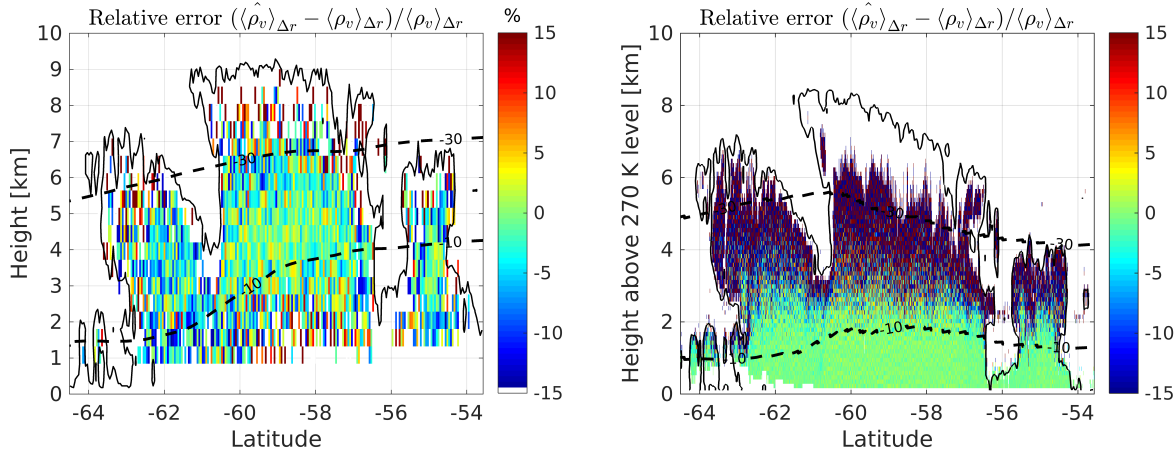
Figure 6. Left panel: relative error in the retrieval of ρ_v for the case study shown in Fig. 3 for a 7-channel space-borne DAR with frequencies as listed in the legend on the top side of Fig. 5. Here $\Delta r = 500$ m and a 5 km along-track averaging has been performed. The dashed lines correspond to the -30°C and -10°C isotherms and the black line corresponds to CloudSat reflectivities of -25 dBZ (roughly indicating the cloud boundaries). Right panel: same as left panel for a 5-tone ground-based DAR with frequencies as listed in the legend on the bottom side of Fig. 5. Here $\Delta r = 120$ m and a 2-minute averaging has been performed.

The relative error in the retrieval of ρ_v for the whole case study shown in Fig. 3 is reproduced in the left panel of Fig. 6. Clearly there are two critical regions: 1) at low temperatures ($\approx T < -30$°C) low values of ρ_v limit the amplitude of the signal (e.g. compare the red curves between the top three small insets in Fig. 5); 2) at warm temperatures ($\approx T > -10$°C) and large CloudSat reflectivities the cumulated attenuation tends to strongly reduce the SNR and therefore [see formula (7)] increase the uncertainty of the reflectivity measurements and as a result of $\gamma(f_j, r)$. In both situations the retrieval becomes inaccurate but such deterioration can be clearly identified by looking at the SNR of the different DAR channels and at the associated error induced in the estimated value of water vapor, $\langle \hat{\rho}_v \rangle_{\Delta r}$.

The same profile has also been used to analyze the performance of a ground-based instrument by assuming that the instrument is located at the $-3°C$ isothermal line and is looking upward. Again tones in the right wing of the absorption band are selected. The simulated reflectivities, shown in the bottom side of Fig. 5, show strong attenuation in the lower troposphere with the tones close to the center of the line reaching the noise level already just above 2 km. The only tones that can penetrate deep into the clouds are the ones that have not enough water vapor signal high up in the troposphere (e.g. the highest three tones at 2.68 km, see bottom small insets in Fig. 5). This demonstrates why, while the accuracy of the retrieval in the lower troposphere is excellent, it deteriorates quickly above 2.5 km. The right panel of Fig. 6 demonstrates the same thing for the whole event: the accuracy of the retrieval is quickly worsening 2/2.5 km above the ground where temperatures decrease to values lower than -15°C. On the other hand, by integrating for periods of the order of 1-2 minutes, ground-based system can achieve extremely accurate results for temperature between 0 and -15°C.

This case study highlights that sounding ice clouds by air-borne or space-borne DAR systems is clearly advantageous with respect to ground systems because regions with low water vapor contents (thus low attenuation) are encountered first. This implies that tones close to the line center can stay well above MDT in the areas where they provide useful information (i.e. at low water vapor contents). The same is not true for ground-based geometry because, unless the temperature at the ground is

5 very cold, large levels of attenuation are experienced by the radar pulse in the lower troposphere.

4 Statistical analysis from CloudSat climatology

The A-Train has provided the first global climatology of ice clouds with a detailed description of ice cloud occurrences, ice microphysics and ice radiative effects (Hong and Liu, 2015). The A-Train ice cloud dataset represents therefore an ideal test-bed to investigate the potential of a DAR system for measuring relative humidity inside ice clouds. The methodology described

10 in Sect. 3 has been applied to ten days of CloudSat data (from 1st to 10th January 2007) to study the performances both of a space-borne and a ground-based DAR system with several channels within the 183.3 GHz absorption band. The ground-based system is assumed to look upward from the height corresponding to the $270\ K$ isothermal level as identified by the ECMWF reanalysis. For any profile with ice water path exceeding 20 g/m^2 the profile of water vapour is retrieved via the DAR technique and, by comparing such value with the assumed one (from ECMWF reanalysis), the relative error on ρ_v is

15 computed. Results are binned according to the CloudSat reflectivity values (above -10 dBZ and -25 dBZ for the space borne and ground-based system, respectively) and the ambient temperatures (above 240 K). Fig. 7 shows the fractional occurrence when the DAR systems provide ρ_v with accuracy better than 3% (i.e. a very valuable information). For the space-borne system there is an optimal region between -5 and 15 dBZ and for temperatures between 250 and 265 K. Results tends to worsen at temperature close to 273 K and at very high reflectivities (a result of the reduced number of tones with signal significantly

20 above the SNR), but also at very cold temperature (a result of the reduced value of the tones further away from the band center) and low reflectivities (a result of the reduced SNR).

For the ground-based system (right panels in Fig. 7) ρ_v is optimally retrieved in the lower troposphere with the quality of the retrieval typically worsening with decreasing temperatures and decreasing reflectivities (due to the reduced SNRs). The only exception is at very large reflectivities, where non linearities of the right hand term in Eq. (6) introduced by Mie and attenuation

25 effects cause larger errors.

We have selected different combinations with 2, 3, ... 5 tones and we have analysed which combinations achieve the best retrieval performances. Results are summarized in Fig. 8. Clearly increasing the number of tones (all with the same sensitivities) is beneficial but the improvement when surpassing four tones is marginal (e.g. compare the 4 with the 5 and 6 tones). On the other hand it is obvious that improving the SNR is generally producing better results via a reduction of the noise in the Z

30 measurements according to Eq.(7). For instance for the 2- and 4-tone curves the impact of the improvement corresponding to a variation of a factor of two in sensitivity (± 3 dB) is illustrated in Fig. 8 by the shading. Note that even when considering DAR configurations with the same duty cycle there is indeed an improvement in water vapor profiling when using four vs
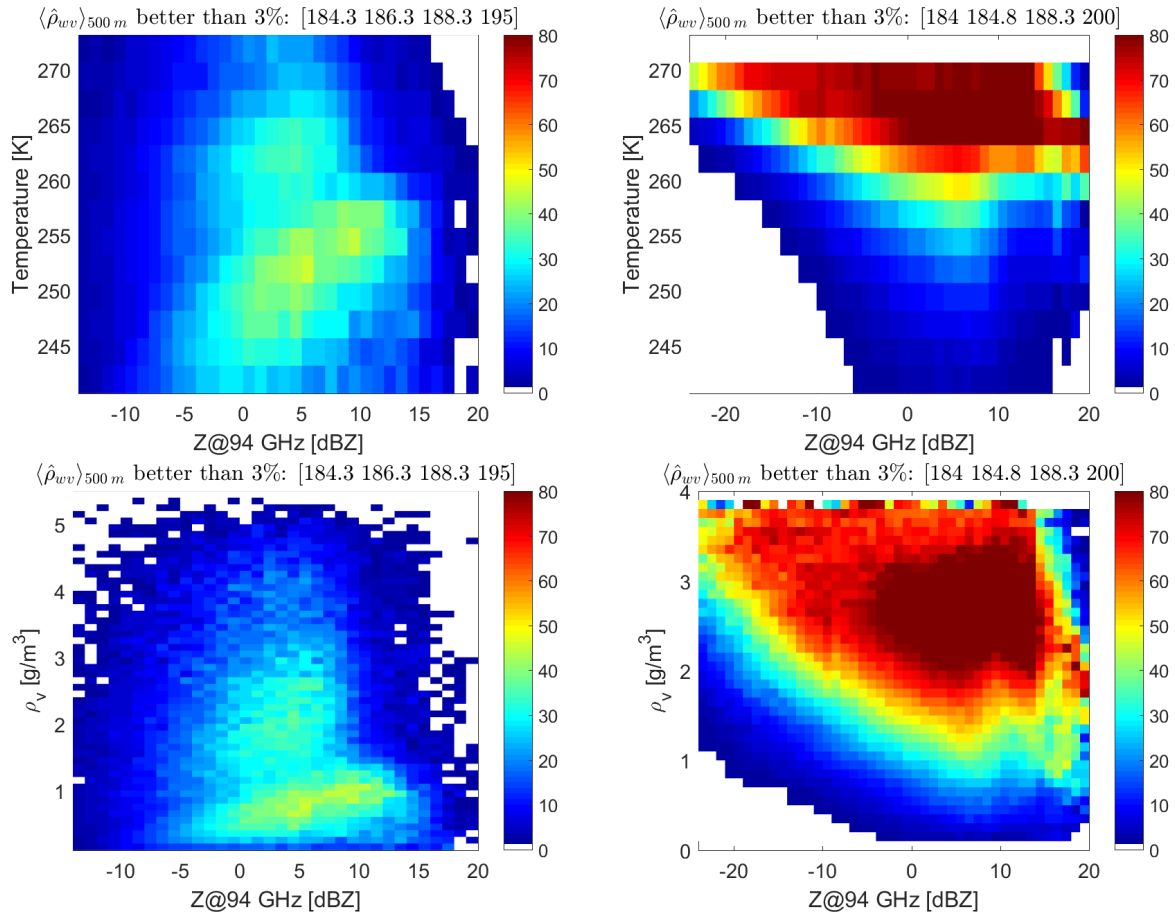
Figure 7. Statistical analysis based on 10 days of CloudSat showing the expected frequency occurrence of retrievals of ρ_v better than 3% for a space-borne system (left) and a ground-based system (with ground temperature of 270 K). Top (bottom) panels: results are clustered using reflectivities vs temperatures (water vapor contents). The specifications of the systems correspond to 4-tone DARs which are optimized for ice cloud studies.

two channels. In fact, doubling the number of channel with the same duty cycle corresponds to averaging half the number of samples, which equates to a reduction of 1.5 dB in sensitivity (so roughly half the range currently shown by the shaded area).

5 Discussion and conclusions

The potential of a multi-frequency differential absorption radar (DAR) system with several tones within the 183.3 GHz water vapor absorption band for profiling water vapour within ice clouds is assessed both for a ground-based and a space-borne
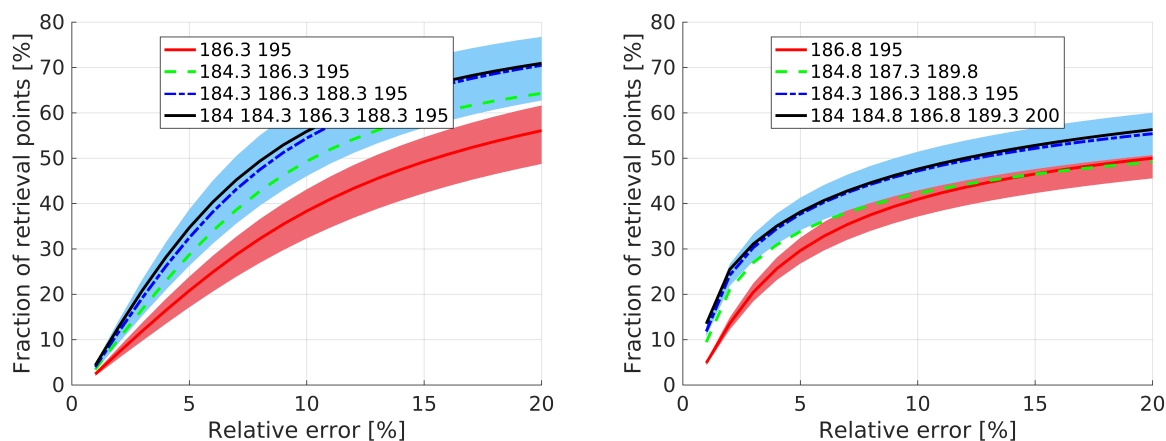
Figure 8. Fraction of retrieval points (y-axis) having errors lower than a given threshold (x-axis) for the space-borne configuration (left) and the ground-based configuration with 2-3-4 and 5 tones. Only the combinations that achieve the best accuracies (as indicated in the legend) are reported. The dashed region indicate results when the sensitivity is increased/decreased by 3 dB. For the space-borne (ground-based) configuration the retrieval is applied only to points corresponding to CloudSat reflectivities exceeding -15 dBZ (-25 dBZ) and temperature exceeding 240 K.

configuration. Realistic ice profiles derived from A-Train observations are inputs of DAR simulations which are used to test the performances of water vapor retrievals based on fitting the line shape via a minimum least square fitting procedure.

Our findings can be summarized as following.

1. With realistic minimum detection thresholds, DARs can provide useful information in thick ice/mixed-phase clouds
5   and they can complement other techniques (e.g. water vapor DIALs, Nehrir et al. (2017)). Four tone DARs seem to be the right balance between complexity (i.e. number of channels) and retrieval performances. In the domain of CloudSat reflectivities above -15 dBZ and $T > 240$ some of the best 4-tone combination allow to retrieve ρ_v with accuracy better than 3% in more than 25% of the cases when ice is present with the best results obtained for ice clouds with reflectivities between -5 and 10 dBZ.

10 2. Ground-based DAR systems can provide excellent profiling of the warmer parts of ice clouds where ρ_v values exceed $1 \ \mathrm{gm}^{-3}$ but they become increasingly less accurate when looking at the cold regions with low moisture. In such areas things are expected to improve when colder ground temperature are considered (here we have simulated a scenario with ground temperature of 270 K). Also scanning options could be considered to increase the differential absorption signal of channels far away from the center of the band by increasing the path length.

15 3. Air-borne or space-borne DAR systems are clearly advantageous with respect to ground systems when looking at regions with low water vapor contents because such regions are encountered first by the radar wave and therefore are affected

by less attenuation. This implies that tones close to the band center can stay well above MDT in the areas where they provide useful information (i.e. at low water vapor contents). The same is not true for ground-based geometry because, unless the temperature at the ground is very cold, large levels of attenuation are experienced by the radar tones close to the band center in the lower troposphere.

4. The selection of the tones is driven by a tradeoff between differential signal and signal. Ideally the attenuation signal should be maximised but if the attenuation is too strong the signal becomes increasingly noisy and ultimately goes below the minimum sensitivity. For ground-based systems it would be ideal to have tones that can be adjusted depending on the atmospheric conditions and latitude/altitude location since, with lower ground temperatures, channels closer to the 183.3 GHz center becomes increasingly useful.

5. The quality of the retrieval can be easily evaluated by considering retrieval errors and χ^2 values that are computed as part of the minimum least square fitting procedure.

6. Transmitting licences are attainable for airborne and ground-based (e.g. in UK DAR tones within the following bands may be allowed: 173.85 to 182 GHz, 185 to 190 GHz, 191.8 to 195.75 GHz, 196.15 to 199.99 GHz with other allowed windows below 173.85) but currently much more unaccessible for space-borne systems since such bands are reserved to passive microwave radiometers. As a first step to assess the potential of the DAR concept for ice cloud studies a ground-based DAR system to be deployed at high latitude/ high altitudes is highly recommended.

Acknowledgements. This work was supported by the European Space Agency under the activity "Multi Frequency Radar Instrument Study", Contract: 4000120689/17/NL/IA. The work by Alessandro Battaglia has been supported by the project Radiation and Rainfall funded by the UK National Center for Earth Observation. This research used the ALICE High Performance Computing Facility at the University of Leicester.

References

Anderson, E.: Statement of guidance for global numerical weather prediction (NWP), Tech. rep., WMO, https://www.wmo.int/pages/
prog/www/OSY/GOS-RRR.html, 2014.

Battaglia, A. and Delanöe, J.: Synergies and complementarities of CloudSat-CALIPSO snow observations, J. Geophys. Res., 118, 721–731,
5   dOI: 10.1029/2012JD018092, 2013.

Battaglia, A. and Kollias, P.: Error Analysis of a Conceptual Cloud Doppler Stereoradar with Polarization Diversity for Better Understanding
Space Applications, J. Atmos. Ocean Technol., 32, 1298–1319, doi: http://dx.doi.org/10.1175/JTECH-D-14-00015.1, 2014.

Battaglia, A., Tanelli, S., Kobayashi, S., Zrnic, D., Hogan, R., and Simmer, C.: Multiple-scattering in radar systems: a review, J. Quant.
Spectrosc. Radiat. Transfer, 111, 917–947, doi:10.1016/j.jqsrt.2009.11.024, 2010.

10   Battaglia, A., Westbrook, C. D., Kneifel, S., Kollias, P., Humpage, N., Löhnert, U., Tyynelä, J., and Petty, G. W.: G-band (140-220 GHz)
atmospheric radars: new frontiers in cloud physics, Atm. Meas. Tech., 7, 1527–1546, doi:10.5194/amt-7-1527-2014, 2014.

Battaglia, A., Dhillon, R., and Illingworth, A.: Doppler W-band polarization diversity space-borne radar simulator for wind studies, Atm.
Meas. Tech., 11, 5965–5979, https://doi.org/10.5194/amt-11-5965-2018, 2018.

Cooper, K. B., Monje, R. R., Millán, L., Lebsock, M., Tanelli, S., Siles, J. V., Lee, C., and Brown, A.: Atmospheric Humidity Sounding
15   Using Differential Absorption Radar Near 183 GHz, IEEE Geosci. Remote Sens. Lett., 15, 163–167, 2018.

Delanoë, J. and Hogan, R.: Combined CloudSat-CALIPSO-MODIS retrievals of the properties of ice clouds, J. Geophys. Res., 115,
doi:10.1029/2009JD012346, 2010.

Durden, S. L., Tanelli, S., Epp, L. W., Jamnejad, V., Long, E. M., Perez, R. M., and Prata, A.: System Design and Subsystem Technology for
a Future Spaceborne Cloud Radar, IEEE Geosci. Remote Sens. Lett., 13, 560–564, 2016.

20   Haddad, Z. S., Sy, O. O., Hristova-Veleva, S., and Stephens, G. L.: Derived observations from frequently-sampled microwave
measurements of precipitation. Part I: Relations to atmospheric thermodynamics, IEEE Trans. Geosci. Remote Sens., 55, doi:
10.1109/TGRS.2017.2671598, 2017.

Hogan, R. J. and Illingworth, A. J.: The Potential of Spaceborne Dual-Wavelength Radar to Make Global Measurements of Cirrus Clouds, J.
Atmos. Ocean Technol., 16, 518–531, doi: http://dx.doi.org/10.1175/1520-0426(1999)016<0518:TPOSDW>2.0.CO;2, 1999.

25   Hogan, R. J. and Westbrook, C. D.: Equation for the microwave backscatter cross section of aggregate snowflakes using the Self-Similar
Rayleigh-Gans Approximation, J. Atmos. Sci., 71, 3292–3301, 2014.

Hogan, R. J., Gaussiat, N., and Illingworth, A.: Stratocumulus Liquid Water Content from Dual-Wavelength Radar, J. Atmos. Ocean Technol.,
22, 1207–1218, doi: http://dx.doi.org/10.1175/JTECH1768.1, 2005.

Hong, Y. and Liu, G.: The Characteristics of Ice Cloud Properties Derived from CloudSat and CALIPSO Measurements, J. Climate, 28,
30   3880–3901, doi: 10.1175/JCLI-D-14-00666.1, 2015.

Illingworth, A. J., Barker, H. W., Beljaars, A., Chepfer, H., Delanoe, J., Domenech, C., Donovan, D. P., Fukuda, S., Hirakata, M., Hogan,
R. J., Huenerbein, A., Kollias, P., Kubota, T., Nakajima, T., Nakajima, T. Y., Nishizawa, T., Ohno, Y., Okamoto, H., Oki, R., Sato, K.,
Satoh, M., Wandinger, U., and Wehr., T.: The EarthCARE Satellite: the next step forward in global measurements of clouds, aerosols,
precipitation and radiation, Bull. Amer. Met. Soc., pp. 1311–1332, doi: http://dx.doi.org/10.1175/BAMS-D-12-00227.1, 2015.

35   Illingworth, A. J., Battaglia, A., Bradford, J., Forsythe, M., Joe, P., Kollias, P., Lean, K., Lori, M., Mahfouf, J.-F., Mello, S., Midthassel, R.,
Munro, Y., Nicol, J., Potthast, R., Rennie, M., Stein, T., Tanelli, S., Tridon, F., Walden, C., and Wolde, M.: WIVERN: A new satellite

concept to provide global in-cloud winds, precipitation and cloud properties, Bull. Amer. Met. Soc., pp. 1669–1687, doi: 10.1175/BAMS-D-16-0047.1, 2018.

Joe, P., Kidd, C., Kollias, P., Tanelli, S., Moisseev, D., Battaglia, A., Koikinen, J., Arbery, G., Deligny, B., Caubet, E., Hudak, D., Stewart, R., Wolde, M., Im, E., Vane, D., Stephens, G., Bennartz, R., Blanchet, J.-P., and Cober, S.: The Polar Precipitation Measurement mis-
5   sion, in: Proc. 6th European Conference on Radar Meteorology and Hydrology: Satellite radar measurements and hydro-meteorological applications, Sibiu, Romania, 6-10 September, 2010, 2010.

Kärcher, B., Dörnbrack, A., and Sölch, I.: Supersaturation Variability and Cirrus Ice Crystal Size Distributions, J. Atmos. Sci., 71, 2905–2926, doi: 10.1175/JAS-D-13-0404.1, 2014.

Kollias, P., Battaglia, A., Tatarevic, A., Lamer, K., Tridon, F., and Pfitzenmaier, L.: The EarthCARE cloud profiling radar (CPR) doppler
10   measurements in deep convection: challenges, post-processing, and science applications, in: Proc. SPIE 10776, Remote Sensing of the Atmosphere, Clouds, and Precipitation VII, vol. 107760R, doi: 10.1117/12.2324321, 2018.

Kummerow, C. D., Barnes, W., Kozu, T., Shiue, J., and Simpson, J.: The Tropical Rainfall Measuring Mission (TRMM) sensor package, J. Atmos. Ocean Technol., pp. 809–817, 1998.

Lebsock, M. D., Suzuki, K., Millán, L. F., and Kalmus, P. M.: The feasibility of water vapor sounding of the cloudy boundary layer using a
15   differential absorption radar technique, Atm. Meas. Tech., 8, 3631–3645, doi:10.5194/amt-8-3631-2015, 2015.

Leinonen, J. and Szyrmer, W.: Radar signatures of snowflake riming: A modeling study, Earth and Space Science, 2, 346–358, doi:10.1002/2015EA000102, 2015.

Leinonen, J., Lebsock, M., Tanelli, S., Suzuki, K., Yashiro, H., and Miyamoto, Y.: Performance assessment of a triple-frequency spaceborne cloud-precipitation radar concept using a global cloud-resolving model, Atm. Meas. Tech., 8, 3493–3517, doi:10.5194/amt-8-3493-2015,
20   2015.

Lhermitte, R.: Attenuation and Scattering of Millimeter Wavelength Radiation by Clouds and Precipitation, J. Atmos. Ocean Technol., 7, 464–479, 1990.

Mace, G. G., Marchand, R., Zhang, Q., and Stephens, G.: Global hydrometeor occurrence as observed by CloudSat: Initial observations from summer 2006, Geophys. Res. Lett., 34, L09808, doi:10.1029/2006GL029017, 2007.

25 Magono, C. and Lee, C.: Meteorological classification of natural snow crystals, J. Fac. Sci., 4, 321–335, 1966.

Millán, L., Lebsock, M., Livesey, N., and Tanelli, S.: Differential absorption radar techniques: water vapor retrievals, Atm. Meas. Tech., 9, 2633–2646, doi:10.5194/amt-9-2633-2016, 2016.

Nehrir, A. R., Kiemle, C., Lebsock, M. D., Kirchengast, G., Buehler, S. A., Löhnert, U., Liu, C.-L., Hargrave, P. C., Barrera-Verdejo, M., and Winker, D. M.: Emerging Technologies and Synergies for Airborne and Space-Based Measurements of Water Vapor Profiles, Surv.
30   Geophys., 38, 1445–1482, https://doi.org/10.1007/s10712-017-9448-9, 2017.

Nils, K., Kneifel, S., Löhnert, U., Kollias, P., Czekala, H., and Rose, T.: A W-Band Radar–Radiometer System for Accurate and Continuous Monitoring of Clouds and Precipitation, J. Atmos. Ocean Technol., 34, 2375–2392, doi: 10.1175/JTECH-D-17-0019.1, 2017.

Oue, M., Kumjian, M. R., Lu, Y., Jiang, Z., Clothiaux, E. E., Verlinde, J., and Aydin, K.: X-band polarimetric and Ka-band Doppler spectral radar observations of a graupel producing Arctic mixed-phase cloud, J. Appl. Meteorol. Climatol., 55, 403–424, 2016.

35 Peral, E., Tanelli, S., Haddad, Z., Sy, O., Stephens, G., and Im, E.: Raincube: A proposed constellation of precipitation profiling radars in CubeSat, in: 2015 IEEE International Geoscience and Remote Sensing Symposium (IGARSS), Milan, pp. 1261–1264, doi: 10.1109/IGARSS.2015.7326003, 2015.

Rosenkranz, P. W.: Correction [to"Water vapor microwave continuum absorption: A comparison of measurements and model" by Philip W. Rosenkranz], Radio Science, 34, 1025–1025, https://doi.org/10.1029/1999RS900020, http://dx.doi.org/10.1029/1999RS900020, 1999.

Roy, R. J., Lebsock, M., Millán, L., Dengler, R., R., R. M., Siles, J. V., and Cooper, K. B.: Boundary-layer water vapor profiling using differential absorption radar, Atm. Meas. Tech., 11, 6511–6523, doi: 10.5194/amt-11-6511-2018, 2018.

5   Sassen, K., Wang, Z., and Liu, D.: The global distribution of cirrus clouds from CloudSat/CALIPSO measurements, Geophys. Res. Lett., 113, doi:10.1029/2008JD009972, 2008.

Skofronick-Jackson, G., Petersen, W., Berg, W., Kidd, C., Stocker, E., Kirschbaum, D., Kakar, R., Braun, S., Huffman, G., Iguchi, T., Kirstetter, P., Kummerow, C., Meneghini, R., Oki, R., Olson, W., Takayabu, Y., Furukawa, K., and Wilheit, T.: The Global Precipitation Measurement (GPM) Mission for Science and Society, Bull. Amer. Met. Soc., doi:10.1175/BAMS-D-15-00306.1, 2016.

10   Stephens, G., Winker, D., Pelon, J., Trepte, C., Vane, D., Yuhas, C., L'Ecuyer, T., and Lebsock, M.: CloudSat and CALIPSO within the A-Train: Ten Years of Actively Observing the Earth System, Bull. Amer. Met. Soc., 99, 569–581, https://doi.org/10.1175/BAMS-D-16-0324.1, 2018.

Sy, O. O., Haddad, Z. S., Stephens, G. L., and Hristova-Veleva, S.: Derived Observations From Frequently Sampled Microwave Measurements of Precipitation. Part II: Sensitivity to Atmospheric Variables and Instrument Parameters, IEEE Trans. Geosci. Remote Sens., 55, 15   2898–2912, 2017.

Tanelli, S., Im, E., Durden, S., and Pak, K.: In-Flight Performance of the CloudSat Radar & L1B processing, CloudSat/CALIPSO Joint Science Team meeting, June 11-14, San Francisco, CA, USA, 2007.

Tanelli, S., Durden, S., Im, E., Pak, K., Reinke, D., Partain, P., Haynes, J., and Marchand, R.: CloudSat's Cloud Profiling Radar After 2 Years in Orbit: Performance, Calibration, and Processing, IEEE Trans. Geosci. Remote Sens., 46, 3560–3573, 2008.

20   Tanelli, S., Haddad, Z. S., Im, E., Durden, S. L., Sy, O. O., Peral, E., Sadowy, G. A., and Sanchez-Barbetty, M.: Radar concepts for the next generation of spaceborne observations of cloud and precipitation processes, in: IEEE Proceedings of Radar Conference, Oklahoma City, OK, 2018.

The Decadal Survey, ed.: Thriving on Our Changing Planet: A Decadal Strategy for Earth Observation from Space, The National Academies Press, 2017.

25   Tridon, F., Battaglia, A., Chase, R., Turk, J., Leinonen, J., Kneifel, S., Mroz, K., Finlon, J., Bansemer, A., Tanelli, S., Heymsfield, A., and Nesbitt, S.: The microphysics of stratiform precipitation during OLYMPEX: compatibility between 3-frequency radar and airborne in situ observations, J. Geophys. Res., 2019.

Verlinde, J., Rambukkange, M. P., Clothiaux, E. E., McFarquhar, G. M., and Eloranta, E. W.: Arctic multilayered, mixed-phase cloud processes revealed in millimeter-wave cloud radar Doppler spectra, J. Geophys. Res. Atm., 118, 199–13,213, doi:10.1002/2013JD020183, 30   2013.

Winker, D. M., Hunt, W. H., and McGill, M. J.: Initial performance assessment of CALIOP, Geophys. Res. Lett., 34, doi:10.1029/2007GL030135, 2007.